Author Manuscript

Author Manuscript

Author Manuscript

Author Manuscript

HHS Public Access

Author manuscript

Genesis. Author manuscript; available in PMC 2018 October 06.

Published in final edited form as:

Genesis. 2017 October ; 55(10): . doi:10.1002/dvg.23071.

Selective expression of eGFP in mouse perivascular astrocytes by modification of the Mlc1 gene using T2A-based ribosome skipping

Jordan J. Toutounchian and **Joseph H. McCarty***

Department of Neurosurgery, The University of Texas M. D. Anderson Cancer Center, Houston, TX 77030, USA

Abstract

Perivascular astrocyte end feet closely juxtapose cerebral blood vessels to regulate important developmental and physiological processes including endothelial cell proliferation and sprouting as well as the formation of the blood-brain barrier (BBB). The mechanisms underlying these events remain largely unknown due to a lack of experimental models for identifying perivascular astrocytes and distinguishing these cell types from other astroglial populations. Megalencephalic leukoencephalopathy with subcortical cysts 1 (Mlc1) is a transmembrane protein that is expressed in perivascular astrocyte end feet where it controls BBB development and homeostasis. Based on this knowledge, we used T2A peptide-skipping strategies to engineer a knock-in mouse model in which the endogenous Mlc1 gene drives expression of enhanced green fluorescent protein (eGFP), without impacting expression of Mlc1 protein. Analysis of fetal, neonatal and adult Mlc1-eGFP knock-in mice revealed a dynamic spatiotemporal expression pattern of eGFP in glial cells, including nestin-expressing neuroepithelial cells during development and glial fibrillary acidic protein (GFAP)-expressing perivascular astrocytes in the post-natal brain. EGFP was not expressed in neurons, microglia, oligodendroglia, or cerebral vascular cells. Analysis of angiogenesis in the neonatal retina also revealed enriched Mlc1-driven eGFP expression in perivascular astrocytes that contact sprouting blood vessels and regulate blood-retinal barrier permeability. A cortical injury model revealed that Mlc1-eGFP expression is progressively induced in reactive astrocytes that form a glial scar. Hence, Mlc1-eGFP knock-in mice are a new and powerful tool to identify perivascular astrocytes in the brain and retina and characterize how these cell types regulate cerebral blood vessel functions in health and disease.

Introduction

Astrocytes are the most abundant cell type in the central nervous system (CNS). Several heterogeneous populations of astrocytes have been identified, based primarily on cell shape, anatomic location, and expression of common biomarkers such as GFAP and the glutamate aspartate transporter (GLAST) (Zhang and Barres, 2010). Fibrous astrocytes are located primarily in white matter regions, protoplasmic astrocytes are found mainly in grey matter, and astrocytes with radial glial-like morphologies are found in the cerebellum (Bergman

Correspondence: Dr. Joseph H. McCarty, Department of Neurosurgery, MD Anderson Cancer Center, Unit 1004, 1515 Holcombe Blvd., Houston, TX 77030. Phone: 713-792-0429; Fax: 713-834-6257; jhmccarty@mdanderson.org.

Author Manuscript Author Manuscript Author Manuscript Author Manuscript

glia) and retina (Muller glia) (Ben Haim and Rowitch, 2017; Freeman, 2010). Furthermore, neurogenic regions of the adult brain contain neural stem cells that express GFAP and display many other astrocyte-like features (Lim and Alvarez-Buylla, 2016). This functional heterogeneity has major implications in specific neuropathologies in which astrocyte dysfunction is involved (Sloan and Barres, 2014). Therefore, to better understand CNS development, physiology and disease there is a significant need to identify and distinguish among the various astrocyte subpopulations.

Perivascular astrocytes intimately associate with endothelial cells, pericytes, and their shared vascular basement membranes within multicellular complexes, or neurovascular units, to regulate the development and homeostasis of the blood-brain barrier (BBB) (Muoio *et al.*, 2014). These perivascular cells extend complex processes with end feet that are estimated to ensheath more than 90% of the abluminal surface of cerebral capillaries (Abbott, 2002). Signals from perivascular astrocyte end feet promote the formation and maintenance of endothelial cell tight junctions and control expression of important BBB transporter proteins (Andreone *et al.*, 2015). In addition, by bridging neurons and blood vessels, perivascular astrocytes respond to the dynamic metabolic demands of the brain by directly influencing local blood supply and nutrient supply (Turner and Adamson, 2011). Loss of normal astrocyte-endothelial cell coupling leads to disruption of the BBB in pathologies such as germinal matrix hemorrhage (Ozduman *et al.*, 2004), age-related neurodegeneration (Zhao *et al.*, 2015) and cancer (Jain *et al.*, 2007). Although there are various proteins such as GFAP and GLAST expressed exclusively in astrocytes, there are currently no specific biomarkers that distinguish the different perivascular astrocytes form other populations of astrocytes in the CNS.

Megalencephalic leukoencephalopathy with subcortical cysts (MLC) is a heritable human disease associated with loss-of-function mutations in the MLC1 gene (Ilja Boor *et al.*, 2006; Leegwater *et al.*, 2001; van der Knaap *et al.*, 1995). Mlc1 is a 38-kDa domain protein and shares sequence homology with K^+ ion channels (Boor *et al.*, 2005). Mlc1 partners with glial cell adhesion molecule (GlialCAM) and both are expressed in distal astroglial end feet are perivascular, subependymal, and subpial sites, indicating important roles at the BBB and the blood-cerebrospinal fluid barrier (Brignone *et al.*, 2015). Brain magnetic resonance imaging (MRI) scans of MLC patients show a diffuse white matter signal, indicating poor ion/fluid balance leading to edema and progressive neurocognitive decline (van der Knaap *et al.*, 1995). Although the exact functions for Mlc1 remain largely unknown, its enriched expression in perivascular astrocytes suggests that the gene and/or protein can be exploited to selectively identify these cells and characterize their functions related to the BBB.

We used T2A ribosome skipping technology to develop a knock-in mouse model in which the endogenous Mlc1 gene drives eGFP expression (Szymczak *et al.*, 2004). In this system, a viral 2A sequence disrupts translation due to the inability of the ribosome to link the glycine and proline residues at its C-terminus, and is thus “skipped”. The resulting individual gene products, Mlc1 and eGFP, are both expressed without perturbing overall levels of Mlc1 protein. Here, we show that Mlc1-driven eGFP expression is enriched in perivascular astrocytes and does not co-localize with other neurovascular unit components, including neurons, endothelial cells, pericytes or other glial cell types. The establishment and

Author Manuscript Author Manuscript Author Manuscript Author Manuscript

characterization of the Mlc1-eGFP transgenic mouse is an important first step to identify and characterize perivascular astrocytes from the CNS. This model may be a key to understanding the genetic and biochemical profiles of perivascular astrocytes and their contributions to blood vessel functions.

Results

Engineering the Mlc1-eGFP knock-in mouse model

Analysis of Mlc1 protein expression by immunohistochemical stains of the P30 mouse brain confirmed perivascular astrocyte expression in the cortex, whereas in the cerebellum Mlc1 protein was enriched in Bergmann glial processes (Fig 1A and S1 Fig). We found that the commercially available antibodies that are amenable for detecting Mlc1 protein by immunohistochemistry are not suitable for fluorescence-activated cell sorting (FACS) to fractionate perivascular astrocytes (data not shown). Furthermore, available mouse models that express fluorescent reporters via astrocyte-specific promoters label multiple types of astrocytes, and do not distinguish perivascular astrocytic populations (Chaboub *et al.*, 2016; Guo *et al.*, 2017). T2A ribosome skipping methodologies were used to develop a knock-in mouse model in which the endogenous Mlc1 gene drives eGFP expression. A BAC (RP23-268N19) was engineered to contain the targeting sequence and a long homology arm extending into exon 12 of Mlc1 (Fig 1B). The reporter cDNA was fused in frame to exon 12 so that eGFP uses the endogenous polyA of Mlc1 to terminate the transcript. The T2A-EGFP was inserted in the open reading frame of the Mlc1 gene after the CAG codon in exon 12 such that the ribosome will translate through the T2A-EGFP sequence, resulting in two proteins (Mlc1 and EGFP) without termination. Termination is initiated at the 3`UTR where the endogenous polyA sequence resides. A Flp-recognition target (FRT)-flanked inverted Neo cassette was inserted downstream of Mlc1 3`UTR sequence to facilitate ES cell screening. Homologous recombination in Flp-expressing ES cells (n=5) was confirmed by genomic PCR (S1 Fig). After Flp-mediated deletion of the neomycin cassette, a FRT site remains in Mlc1-eGFP/+ heterozygous and Mlc1-eGFP/Mlc1-eGFP homozygous mice. Absence of the Neo cassette was used to screen F1 mice using conventional PCR-based genotyping methods. Heterozygotes contain both the wild type 314 bp PCR product and a higher molecular weight band of 399 bp due to the remaining FRT site. In homozygotes, only the upper 399 bp band is detected. The genotypes of wild type, heterozygotes and homozygotes can be differentiated by genomic PCR using tail snip DNA (Fig 1C). Litters were average size (5–8 pups) and knock-in pups were born in expected Mendelian ratios (data not shown). Adult heterozygous and homozygous mice display fertility and have survived for six months without obvious phenotypes.

Mlc1 drives expression eGFP in perivascular astrocytes

Expression of eGFP in unfixed brain tissue was not readily detectable (data not shown); therefore, anti-GFP antibodies were used to analyze expression patterns of eGFP in Mlc1-eGFP knock-in mice. We analyzed P30 wild type control and Mlc1-eGFP/+ heterozygous brains and focused on the cortex, hippocampus and cerebellum (Fig 2). Double immunofluorescence labeling was performed using anti-eGFP antibodies in combination with antibodies recognizing proteins specifically expressed in astrocytes, neurons, or

Author Manuscript Author Manuscript Author Manuscript Author Manuscript

vascular endothelial cells. Mlc1-regulated eGFP expression in astrocytes was apparent in the different regions of the brain, as evidenced by overlap with GFAP. Control wild type littermates showed no expression of eGFP (Fig 2A–C; a–g). Neurons and vascular endothelial cells were negative for eGFP expression, as confocal analysis showed clear demarcation between $eGFP^+$ cells, $NeuN^+$ neurons and $CD31^+$ endothelial cells (Fig 2A–C; h–k and l–o, respectively). As expected for perivascular astrocytes, we observed robust eGFP expression in $GFAP^+$ astrocyte processes near cerebral vessels (Fig 2A–C; panel o and S2 Fig). Further analysis of the adult cortex showed near complete overlap of GFP and GFAP in astrocytes juxtaposing blood vessels (Fig 2D; a–g). To further distinguish $eGFP^+$ cells from other cell types of the brain, antibodies were used to analyze additional neurovascular biomarkers (Fig 3A), including calbindin (neurons, a–c), aquaporin-4 (endothelial cells and astrocytes, d–f), NG2 (pericytes and oligodendroglia, g–h), myelin basic protein (MBP, oligodendroglia, i–l), neurofilament (neurons, Fig 3B, a), and laminin (vascular basement membranes, Fig 3B, c). Double immunofluorescence labeling for these proteins in combination with anti-GFP antibodies did not reveal co-expression in $eGFP^+$ cells (Fig 3A–B). Immunohistochemistry analysis of fixed brain tissue sections showed similar patterns of eGFP and Mlc1 protein expression in Mlc1-eGFP mice (Fig 3C, a, b), but not in wild type control sections (Fig 3C, e, f). Control IgGs stains also confirmed antibody specificities (Fig 3C, c,d).

EGFP is expressed in neuroepithelial cells of the developing brain

Neuroepithelial cells and radial glia are multipotential cell types that are enriched in germinal centers of the embryonic brain where they regulate neuronal migration (Metin *et al.*, 2008) and also serve as guides for angiogenic blood vessels (McCarty, 2009; Segarra *et al.*, 2015). To analyze the expression patterns of Mlc1-regulated eGFP in the developing brain, we analyzed E14 and E16 embryonic brain sections with anti-GFP antibodies in combination with anti-CD31 to identify vascular endothelial cells and anti-nestin to identify neuroepithelial cells and radial glia (Fig 4). In horizontal sections through the E14 brain, $eGFP^+$ cells with radial morphologies were detected in forebrain subventricular zones, including the ganglionic eminences (Fig 4A–C). EGFP expression clearly overlapped with nestin, but was distinct from CD31-expressing endothelial cells and Tuj1-expressing neurons, (Fig 4B). In additional E16 sagittal brain sections, eGFP staining was evident in cells within the developing hippocampal dentate gyrus (DG), and this also overlapped with nestin expression. There was no coincident localization of eGFP and Tuj1 or eGFP and CD31 in the hippocampus (Fig 4D, E).

We next analyzed the hippocampus, cerebellum and cortex of wild type and heterozygous P0, P3, and P7 neonatal littermates using anti-eGFP and anti-GFAP double fluorescent labeling (Fig 5). In the developing P0 and P3 hippocampus, eGFP expression was detected in cells that, based on their polarity, were likely migrating away from the subgranular layer (Fig 5A,C). P7 brain sections showed an increase in $eGFP^+$ cell numbers that were clearly defining the hippocampal DG (Fig 5A, k,l). Striking patterns of $eGFP^+$ cells were detected within the P0, P3 and P7 mouse cerebellum (Fig 5B). These $eGFP^+$ cells are likely Bergmann glia and/or glial progenitors, which are specialized cerebellar astrocytes that establish radial processes that facilitate granule neuron migration during post-natal

Author Manuscript Author Manuscript Author Manuscript Author Manuscript

cerebellar development and maintain cerebellar architecture into adulthood (Buffo and Rossi, 2013). In addition, anti-CD31 immunostaining was performed to analyze the vasculature during neonatal mouse brain development at P0, P3 and P7. Similar to analysis of adult brain samples (P30, Figs. 2–3), processes emanating from $eGFP^+$ cell bodies showed intimate contacts with cerebral blood vessels throughout the P0, P3 and P7 brain samples (Fig 5D–F).

Analysis of Mlc1 and eGFP expression in cultured mouse astrocytes

We next cultured primary astrocytes from P3 wild-type control, Mc1-eGFP/+ heterozygote, and Mc1-eGFP/Mc1-eGFP homozygote littermates (n=3 mice per genotype) and analyzed these cells *in vitro*. Genotypes of pups were confirmed using tail snip DNA and genomic PCR. Detergent-soluble lysates from astrocyte cultures were immunoblotted with anti-GFP, anti-GFAP, and anti-Mlc1 antibodies. Our results reveal that eGFP was not present in wild type control cells, while cells isolated from Mc1-eGFP/+ heterozygous and Mc1-eGFP/Mc1-eGFP homozygous mice showed abundant eGFP expression (Fig 6A–B). There was a greater than two-fold increase of eGFP expression in Mc1-eGFP/Mc1-eGFP homozygous cells as compared to Mc1-eGFP/+ cells (Fig 6B). EGFP expression was not detected in wild type control astrocytes. Anti-Mlc1 immunoblots revealed robust Mlc1 protein expression in cultured astrocytes (Fig 6A). The apparent molecular weight of Mlc1 protein is slightly higher in cells isolated from homozygous mice versus wild type control cells, due to residual 2A peptide sequences covalently linked to the C-terminus of the Mlc1 protein. This is also apparent in whole-brain lysates (Fig 1D). Since heterozygous mice have one wild type copy of Mlc1, a lower molecular weight band exists in addition to the higher molecular weight Mlc1-2A peptide (Fig 6A; indicated by an asterisk).

In addition to the immunoblotting results, we performed immunofluorescence staining on adherent astrocytes (Fig 6C). There was no detectable eGFP signal in wild type astrocytes, compared to high levels of expression in Mc1-eGFP heterozygous and homozygous cells (Fig 6C). Integrated density quantitation showed that homozygous cells had more intense staining for eGFP as compared to heterozygous astrocytes (Fig 6D). Nearly 100% of cells, regardless of Mlc1-eGFP genotype, expressed GFAP (Fig 6C, d–f). When quantifying the number of cells positive for both eGFP and GFAP, Mc1-eGFP/+ and Mc1-eGFP/ Mc1-eGFP cultures both showed similar ratios of $eGFP^+/GFAP^+$ cells. Wild type control cells did not stain positive with anti-GFP antibodies (Fig 6D). Additional immunostains were performed on wild type astrocytes using control IgGs generated in chicken, mouse, goat and rabbit (S4 Fig). We also performed double immunostaining using eGFP and Mlc1 antibodies in all astrocytes. Our results show that cells positive for eGFP also expressed Mlc1 at a near 1:1 ratio (S4 Fig).

EGFP is upregulated in reactive astrocytes in response to cortical injury

Activation and recruitment of astrocytes is involved in tissue ‘repair’ in response to brain pathologies (Liddelow and Barres, 2016). Reactive astrogliosis is characterized by changes to astrocyte gene expression and morphology at the site of an acute injury which, depending on severity, can trigger glial scarring (Sofroniew, 2009). Given that brain injury often is associated with increased BBB permeability, hypoxia and neoangiogenesis, we hypothesized

Author Manuscript Author Manuscript Author Manuscript Author Manuscript

that Mlc1-eGFP expression would be activated in astrocytes after injury. Therefore, we induced cortical injuries in adult wild type and Mlc1-eGFP heterozygous mice. Brains were collected and analyzed at three and seven days after experimental injury (Fig 7A). The progression in reactive astrogliosis in control and Mlc1-eGFP mice as revealed by double immunofluorescence labeling for eGFP and GFAP over the course of seven days is shown in Figure 7. In Mlc1-eGFP/+ mice we detect increased GFAP expression in reactive astrocytes at 3 days and 7 days post-injury, with apparent co-localization with eGFP around the wound site (Fig 7B). In non-wounded mice (day zero control; Fig 7B, a–d), as well as in the opposite non-injured hemisphere of experimental mice (data not shown), there were no indications of reactive gliosis. We performed double immunostaining for eGFP in combination with CD31 or the microglial marker IBA-1 on day seven brain sections from wild type control (data not shown) and Mlc1-eGFP mice (Fig 7C, D). Blood vessels positive for CD31 (Fig 7C) showed increased diameters and abnormal morphologies near the site of injury, with close juxtaposition of GFAP-expressing astrocytes. IBA-1 staining showed that the activation of microglia, much like GFAP-expressing astrocytes, was significantly enhanced following brain injury at days 3 and 7 (Fig 7D). However, in contrast to GFAP, IBA-1 protein signals did not co-localize with eGFP, suggesting a clear distinction between Mlc1 expression in reactive astrocytes and reactive microglial populations in the injured brain.

Analysis of Mlc1-eGFP expression in retinal vascular development

Retinal astrocytes provide important functions including guidance of angiogenesis and induction of the blood-retinal barrier (Fruttiger, 2007). During the first post-natal week of retinal development in mice, angiogenic blood vessels form a primary vascular plexus by sprouting along a pre-formed network of GFAP-expressing retinal astrocytes (Gerhardt *et al.*, 2003). Since Mlc1 is implicated in the regulation of water and ion balance in the developing brain, we hypothesized that Mlc1-eGFP would be similar expressed within the retinas of developing mice. Whole mounted retinas at P0 (Fig 8A), P3 (Fig 8B) and P7 (Fig 8C) showed progressively upregulated levels of eGFP expression and levels of eGFP remained high in adult retinal samples (S3 Fig). EGFP expression showed clear overlap with GFAP, and there was also close juxtaposition between $eGFP^+$ cells and CD31-expressing retinal endothelial cells. Interestingly, as blood vessels formed a more elaborate vascular network between P3 and P7 (Fig 8B, C), eGFP expression levels also showed a concomitant increase. These findings suggest that as retinal vascular development progresses, the Mlc1 protein is involved in the regulation of blood vessel complexity and/or the formation of the blood-retinal barrier.

Lastly, one reason for developing the Mlc1-eGFP model was to be able to distinguish perivascular cells from other astrocytic cell types and analyze their unique genetic and biochemical properties. Along these lines, we attempted to fractionate cells from wild type control or Mlc1-eGFP P30 homozygous littermates. Cerebral cortices were dissected, enzymatically dissociated and eGFP-expressing cells were fractionated from bulk cell mixtures using FACS. We could clearly distinguish $eGFP^+$ cells from homozygous brains, but not from wild type brains (Fig 9). Approximately 1% of the bulk cortical cell population expressed low, but detectable levels of eGFP, supporting our immunofluorescence data

Author Manuscript Author Manuscript Author Manuscript Author Manuscript

showing that eGFP is expressed in sub-populations of astrocytes in most regions of the brain and retina. These results demonstrate the novelty of the Mlc1-eGFP mouse model for not only identifying perivascular astrocytes *in situ*, but also for fractionating these cells *in vitro* to distinguish their functions in regulating the development and homeostasis of the BBB.

Discussion

Here we report the generation and initial characterization of a new genetically engineered mouse model that expresses eGFP in perivascular astrocytes. EGFP-expressing cells were detected in the cerebral cortex, hippocampus and cerebellum as well as other regions of the neonatal and adult brain. Perivascular $eGFP^+$ expression were also associated with angiogenic blood vessels in the developing retina. To date, we know of no mouse models that demarcate perivascular astrocytes from other astroglial cell populations in the CNS. Aside from the specialized Bergmann glia in the cerebellum, $eGFP^+$ cell processes in other regions of the brain closely juxtaposed blood vessels as evident by proximity to CD31-expressing endothelial cells and laminin-expressing vascular basement membranes. We also confirmed this pattern by using other astrocytic end feet markers (*i.e.*, AQP4), which is also expressed in cerebral endothelial cells (Nagelhus *et al.*, 2004; Yao *et al.*, 2014). EGFP was present in astrocytic cell bodies and processes that contacted blood vessels.

Various genetically engineered mouse models have been generated that label multiple population of astrocytes in the brain. For example, GFP expression by the Aldh1l1 promoter labels most astrocytes in the brain (Gong *et al.*, 2003). Tamoxifen-inducible Cre models are also available that allow for astrocyte-specific reporter expression or gene deletion (Yang *et al.*, 2015). Combined approaches using fluorescent reporter models and antibody-based cell sorting methods have fractionated different astrocyte populations based on gene expression, but it is unclear if perivascular astrocyte pools have been identified using these methods (Chaboub *et al.*, 2016; John Lin *et al.*, 2017). Our Mlc1-eGFP mice represent the first model that enables specific identification of perivascular astrocytes based on expression of an Mlc1-driven eGFP reporter. Our mice, which retain an intact Mlc1 gene and normal Mlc1 protein levels, have advantages over a recently described Mlc1−/− mutant model in which GFP was used to replace exons in the endogenous Mlc1 gene leading to mice with MLC-like neurological deficits (Dubey *et al.*, 2015).

Astrocytes arise from neuroepithelial and radial glial progenitor cells within ventricular zones of the developing brain (Gallo and Deneen, 2014). When we investigated the expression of Mlc1-eGFP during mid-stage to late-stage embryonic development (E14 and E16), the expression patterns closely overlapped with nestin in the ganglionic eminences. These transient structures contain abundant radial glial and neuroepithelial progenitor cells that give rise to neurons that populate the cortex (Anthony *et al.*, 2004). Indeed, immunofluorescence analysis of the developing cerebellar cortex in P0, P3 and P7 pups showed $eGFP^+$ cells, apparently migrating away from the ventricular zone. In the developing cerebellum, granule cell precursor populations migrate along established Bergmann glia fibers and form the inner granular layer, which can be seen in the fully developed cerebellum (Xu *et al.*, 2013). Based on eGFP expression patterns, both embryonic and postnatal developmental patterns observed in Mlc1-eGFP mice recapitulate classical studies

Author Manuscript Author Manuscript Author Manuscript Author Manuscript

investigating neurogenesis during CNS development (Noctor *et al.*, 2001). Importantly, the eGFP expression in newly generated neural cells is transient during development, since analysis of adult mice show more specific expression in perivascular astrocytes.

Following traumatic brain injury, both astrocytes and microglia become activated and contribute to glia scar formation (Eng and Ghirnikar, 1994; Pekny and Nilsson, 2005). This likely facilitates the creation of cellular barrier to prevent blood vessel leakage from causing damage to the surrounding tissue (Bush *et al.*, 1999). We found that Mlc1-eGFP expression followed a similar spatial and temporal expression profile as GFAP upregulation. Astrocyte hypertrophy is postulated to be an important neuroprotective and/or regenerative mechanism (Anderson *et al.*, 2016). Targeting reactive astrocytes through various loss-of-function transgenic models has revealed that any disruption in glial scar formation increases lesions, demyelination and death of neurons, as well as extend recovery time of brain tissue (Ribotta *et al.*, 2004). In contrast, IBA-1 staining of microglia did not overlap with eGFP, suggesting that Mlc1 gene expression correlates with astrocyte-dependent repair following brain injury. A recent study monitoring the step-wise activation of both microglia and astrocytes determined that microglia-derived cytokines were responsible for the activation of neuroprotective astrocytes during and after CNS trauma (Shinozaki *et al.*, 2017). This raises interesting and important questions with regard to what stimulates the induction of Mlc1-eGFP in reactive astrocytes, and whether Mlc1 may contribute to the health and/or recovery of the injured brain.

In summary, the Mlc1-eGFP knock-in mouse model serves as an excellent system to study Mlc1 gene expression in perivascular astrocytes and its role in regulating the BBB and other glial-regulated vascular processes. Isolation of cells from the Mlc1-eGFP knock-in model followed by transcriptome sequencing and metabolic profiling will help to clarify and define the genomic, molecular, and secretory properties that distinguish perivascular astrocytes from other astroglial cell types in the CNS. In addition to enabling fractionation of perivascular cells from the brain based on eGFP expression, similar experimental approaches could be used to inducibly delete loxP-flanked genes selectively in perivascular cells; for example, by engineering Mlc1 to regulate expression of a tamoxifen-responsive Cre recombinase. Effects of specific astrocyte-expressed genes on vascular development, BBB homeostasis, and reactive gliosis can be analyzed. Alternatively, breeding Mlc1-eGFP mice with other models containing mutated genes of interest will enable analysis of how specific pathways control perivascular astrocyte behaviors in the CNS. These future studies will help strengthen our overall understanding of the importance and contributions of perivascular astrocytes in both development and disease.

Materials and Methods

Experimental mice

All mouse experiments were reviewed and approved prior to animal use under the guidance of the Institutional Animal Care and Use Committee (IACUC) and the MD Anderson Subcommittee on Animal Studies, both AAALAC accredited institutions. To generate the Mlc1-eGFP knock-in model, a 9.9 kb region used to construct the targeting vector was first sub-cloned from a positively identified C57bl/6 BAC clone (RP23-268N19) using

Author Manuscript Author Manuscript Author Manuscript Author Manuscript

homologous recombination techniques. The region was designed such that the long homology arm extends 6.4 kb 5' to the exon 12 of Mlc1 gene and the eGFP reporter is fused in frame to exon 12 so that eGFP uses the endogenous polyadenylation tail of Mlc1 to terminate the transcript. Flp-expressing embryonic stem (ES) cells were verified for deletion of the neomycin cassette. Two different clones were microinjected into C57bl/6 mice, generating chimeras with high percentage agouti coat color. Subsequent breeding with wild-type C57bl/6 mice produced heterozygous Mlc1-eGFP mice. Tail DNA was analyzed as described below from pups with agouti or black coat color.

Genotyping identification of Mlc1-eGFP embryos, pups and adults was performed using genomic PCR screening with DNA isolated form tail snips. Oligonucleotides used to confirm insertion and subsequent deletion of the neo cassette (forward primer NDEL1: 5'-TGG GCT TTC AGG ACC AGA ATG AGG -3' and reverse primer NDEL2: 5'-ACT GGT GAT CTA GTC TTT ACT CAC AGG GG -3'). The PCR reaction mix comprised 12.5 uL 2× MangoMix (Bioline Reagents Ltd.; London, UK), 11 μL dH2O, 0.25 μL of each primer (1 μM) and 1 μL sample DNA using the following PCR amplification protocol: hot start at 94°C and held for 2 min; 94°C 30 s, 60°C 30 s, 72°C 1 min for 30 cycles; and held at 4°C upon completion. The PCR products were run on a 2% agarose gel with a 100 bp ladder as reference.

Immunofluorescence and immunohistochemistry

Adult mice were anesthetized and fixed by perfusion with 4% paraformaldehyde (PFA). Adult brains were removed and post-fixed for 24 hours. Embryonic and neonatal brains were dissected and immersed in 4% PFA for 24 hours. PFA-fixed adult and neonatal brains were embedded in 4% agarose and sagittally sectioned. Embryonic (E)14 heads/brains were left intact and embedded in 4% low-melt agarose and sectioned along the horizontal axis. E16 sagittal sections were obtained after removing the brain from the partially developed skull and embedding in 4% low-melting agarose. All sectioning was performed with a vibratome set at a thickness of 100 μm per slice. Antibody names, species of origin, vendor catalog numbers, applications used herein, and dilutions are detailed in S1 Table.

Immunofluorescence staining of adult, neonatal, and embryonic mouse brains was performed using PFA-fixed vibratome sections. Briefly, sections were blocked and permeabilized with 0.5% Triton-X-100 containing TBS (TBST) with 10% normal donkey serum for one hour at room temperature with gentle agitation. Primary antibodies were diluted in same blocking buffer and incubated at 4°C overnight. Brain sections were washed three times in 0.5% TBST for one hour per wash. Secondary antibodies were incubated in TBST blocking buffer for two hours at room temperature. Sections were again washed three times in TBST wash buffer for one hour. DAPI was separately added in TBS buffer and incubated with tissue for five minutes. Sections were washed once in TBS and mounted on pre-treated microscope slides and sealed using Vectashield (Vector Laboratories, Inc., Burlingame, Ca) mounting media. Slides were kept at 4°C short-term until imaging. Formalin-fixed paraffin embedded (FFPE) tissue was subjected to immunohistochemistry as previously described (Tchaicha *et al.*, 2011).

Author Manuscript Author Manuscript Author Manuscript Author Manuscript

Retinal whole-mount immunofluorescence analysis

Enucleated eyes from P0, P3, P7, and P30 mice underwent immediate fixation in ice-cold 4% PFA in PBS for one hour and washed three times in ice-cold PBS. Retinas were carefully isolated under a Leica S6E dissecting stereomicroscope (Leica Microsystems, Buffalo Grove, IL) and mounted onto microscope slides. Whole retinas were permeabilized and blocked in 0.3% PBST, 0.2% bovine serum albumin (BSA) and 5% normal donkey serum for one hour at room temperature. Primary antibodies against GFAP, eGFP and CD31 were diluted in the blocking buffer and incubated overnight at 4°C. Retinas were then washed three times in PBST for 20 minutes. Secondary antibodies against primary host species were diluted in blocking buffer, added to retinas, and incubated at room temperature for two hours. Retinas were again washed three times in PBST for 20 minutes and sealed under coverslips using Vectashield mounting medium (Vector Laboratories, Inc.) and stored at 4°C until imaging.

Image Acquisition

Immunofluorescence images were acquired using an Olympus FLUOVIEW FV1000 confocal laser scanning microscope. Multi-dimensional acquisition was carried out using Z-stacks with < 2 μm slicing intervals at a scan rate of 12.5 us/pixel with a resolution of at least 800 × 800 pixels per slice and digitally compiled in FV10-SW (ver. 3.1a). Image acquisition parameters including exposure time, laser power, gain, and voltages were fixed for each imaging channel. 5× images of whole brains were obtained using a Zeiss AxioImager Z1 fluorescence microscope (Carl Zeiss Microscopy; Oberkochen, Germany) with a Zeiss Axiocam 506 camera. Images were acquired in the Zen 2 (ver. 2.0) software. Images were digitally stitched together in Adobe Photoshop CC 2015 (Adobe Systems, Inc.). LUT enhancements for both confocal and fluorescence images were performed in Photoshop (Adobe Systems, Inc.) for visual clarity purposes only. Immunohistochemistry-labeled images were captured using a Zeiss Axio Scope.A1 light microscope (Carl Zeiss Microscopy).

Isolation and analysis of primary brain astrocytes from Mlc1-eGFP knock-in mice

Primary mouse astrocytes were cultured as described previously (McCarty *et al.*, 2005). Briefly, mouse pups at post-natal day three (P3) were genotyped, sacrificed and whole brains were removed and subjected to enzymatic dissociation in a papain-containing buffer (Miltenyi Biotec, #130-095-942; Bergisch Gladbach, Germany). Dissociated cells at high density were resuspended in low-glucose Dulbecco's Modified Eagle's Medium (DMEM) (Hyclone; Logan, UT) containing 10% fetal bovine serum (FBS) with 1% penicillin/streptomycin and seeded to laminin (Sigma) coated dishes. Adherent astrocytes were cultured to confluence for seven days and passaged no more than three times prior to any experimentation.

Cultured astrocytes were analyzed by immunoblotting after SDS-PAGE as previously described (Toutounchian *et al.*, 2017). Whole cell lysates were collected under normal culture conditions in 1% NP-40 (50 mM Tris-HCl pH 8.0, 150 mM NaCl) lysis buffer with protease and phosphatase inhibitor tablets (Roche; Indianapolis, IN). Total protein was measured by BCA assay (Pierce) then denatured at 95°C for five minutes in 5× SDS loading

Author Manuscript Author Manuscript Author Manuscript Author Manuscript

buffer containing 2.5% 2-mercaptoethanol (Sigma) and 15 μg of protein was resolved on 10% Tris-glycine gels. Immunoblotting was performed with nitrocellulose membranes (Bio-Rad), blocked using Odyssey TBS-based blocking buffer (LI-COR), and then incubated with specific primary antibodies diluted in blocking buffer supplemented with 0.1% Tween-20 overnight at 4°C. Target proteins were normalized to total cellular/housekeeping protein, α-tubulin (LI-COR). Secondary antibodies (IRDye 800CW goat anti-rabbit and IRDye 680RD goat anti-mouse) (LI-COR) were incubated in the dark at room temperature for 40 minutes. Dual-channel infrared scan and quantitation of immunoblots were conducted using the Odyssey CLx infrared imaging system with Image Studio (Ver. 5.2) (LI-COR).

Passaged astrocytes were seeded onto laminin coated glass chamber slides (Lab-Tek™ II Chamber Slide™ System, ThermoFisher; Waltham, MA) and cultured overnight to allow for sufficient adherence. Cells were washed once with cold PBS and fixed in 4% PFA for 15 minutes. Non-specific protein was blocked using 10% normal donkey serum in 0.1% PBS-(T)ween-20. Primary antibodies directed against eGFP, GFAP, Mlc1, and appropriate IgG controls were incubated overnight at 4°C. Cells were washed with 0.1% PBST three times for 15 minutes. Secondary antibodies against primary host species were diluted in blocking buffer and incubated with slides at room temperature for two hours. Cell were washed with PBS-T three times for 15 minutes. DAPI (1 μg/mL) was added to the cells for five minutes and washed three times in PBS. Coverslips were mounted onto slides with Vectashield mounting medium (Vector Laboratories, Inc.) and stored at 4°C in the dark until imaging. The number of $eGFP^+/GFAP^+$ cells were calculated from at least 6 fields of view from three individual experiments ($n > 100$ cells). Integrated densities of $eGFP^+/GFAP^+$ cells were measured to analyze differences across wild type, Mlc1-eGFP/+, and Mlc1-eGFP/Mlc1-eGFP astrocytes (n=5 fields/experimental group from at least 100 cells total).

Brain injury model

Cortical stab wounds were generated in both wild type and heterozygous (Mlc1-eGFP/+) littermates to analyze astrocytic activation and recruitment to the site of injury (Pekny and Nilsson, 2005). A single incision made from the anterior pole of the skull to the posterior ridge. A wound was made through the pial surface at the initial stereotactic point of entry (1.5 mm rostral, 1.5 mm anterior) using a sterile scalpel blade (no. 11). Three and seven days after the injury, mice in each group (n=3 mice per genotype and time point) were anesthetized, cardiac-perfused with 4% PFA/PBS, and brain sections were analyzed. Resting/uninjured brains of wild type control and Mlc1-eGFP/+ littermates were used as the day zero control.

Brain dissociation and FACS analysis of eGFP-expressing cells

Adult mice (P30) were genotyped, sacrificed and cerebral cortices were excised and subjected to enzymatic dissociation in a papain-containing buffer (Miltenyi Biotec). Dissociated live (unfixed) cells from wild type and homozygous knock-in brains were resuspended at high density (20 million cells/ml) in PBS containing 10% FBS and analyzed for eGFP expression using a BD FACSAria III flow cytometer (BD Biosciences, San Jose, CA). Populations of eGFP positive cells were determined after gating with cell suspensions from wild type controls.

Author Manuscript Author Manuscript Author Manuscript Author Manuscript

Statistical analyses

All data represented herein were performed in replicates of three or more and are presented as the mean ± standard deviation (SD), unless otherwise indicated. Differences among groups were analyzed using one-way analysis of variance (ANOVA). When overall analysis revealed significance among groups, means were compared and tested using Tukey's post-hoc analysis. Statistical significance was set at $P < 0.05$. All statistical analyses were performed in SigmaPlot 12.0 software (Systat Software, Inc., San Jose, CA).

Supplementary Material

Refer to Web version on PubMed Central for supplementary material.

Acknowledgments

We thank Caroline C. Carrillo and Verlene K. Henry (Brain Tumor Center, MD Anderson Cancer Center) for their assistance with the cortical injury model. Additionally, we would like to thank Dr. Je Hoon Seo, D.V.M, Ph.D. (Chungbuk National University College of Medicine, South Korea) for technical assistance with ocular cryostat sectioning.

Funding Support: This work was supported by grants to J.H.M. from NIH/NINDS (R01NS087635 and R01NS078402), the Cancer Prevention and Research Institute of Texas (RP140411), and in part by an NIH/NCI SPORE in Brain Cancer (P50CA127001).

Abbreviations

BBB	Blood-brain barrier
MLC	megalencephalic leukoencephalopathy with subcortical cysts
T2A	Thoseaasigna virus 2A
BAC	bacterial artificial chromosome
eGFP	enhanced green fluorescent protein
WT	wild-type
HET	heterozygote
HOM	homozygote
DAPI	4', 6-diamidino-2'-phenylindole
Flp	flippase
FRT	Flp-recognition target

References

Abbott NJ. Astrocyte-endothelial interactions and blood-brain barrier permeability. J Anat. 2002; 200:629–638. [PubMed: 12162730]

Anderson MA, Burda JE, Ren Y, Ao Y, O'Shea TM, Kawaguchi R, Coppola G, Khakh BS, Deming TJ, Sofroniew MV. Astrocyte scar formation aids central nervous system axon regeneration. Nature. 2016; 532:195–200. [PubMed: 27027288]

Author Manuscript Author Manuscript Author Manuscript Author Manuscript

Andreone BJ, Lacoste B, Gu C. Neuronal and vascular interactions. Annu Rev Neurosci. 2015; 38:25–46. [PubMed: 25782970]

Anthony TE, Klein C, Fishell G, Heintz N. Radial Glia Serve as Neuronal Progenitors in All Regions of the Central Nervous System. Neuron. 2004; 41:881–890. [PubMed: 15046721]

Ben Haim L, Rowitch DH. Functional diversity of astrocytes in neural circuit regulation. Nat Rev Neurosci. 2017; 18:31–41. [PubMed: 27904142]

Boor PK, de Groot K, Waisfisz Q, Kamphorst W, Oudejans CB, Powers JM, Pronk JC, Scheper GC, van der Knaap MS. MLC1: a novel protein in distal astroglial processes. J Neuropathol Exp Neurol. 2005; 64:412–419. [PubMed: 15892299]

Brignone MS, Lanciotti A, Camerini S, De Nuccio C, Petrucci TC, Visentin S, Ambrosini E. MLC1 protein: a likely link between leukodystrophies and brain channelopathies. Front Cell Neurosci. 2015; 9:66.

Buffo A, Rossi F. Origin, lineage and function of cerebellar glia. Prog Neurobiol. 2013; 109:42–63. [PubMed: 23981535]

Bush TG, Puvanachandra N, Horner CH, Polito A, Ostenfeld T, Svendsen CN, Mucke L, Johnson MH, Sofroniew MV. Leukocyte infiltration, neuronal degeneration, and neurite outgrowth after ablation of scar-forming, reactive astrocytes in adult transgenic mice. Neuron. 1999; 23:297–308. [PubMed: 10399936]

Chaboub LS, Manalo JM, Lee HK, Glasgow SM, Chen F, Kawasaki Y, Akiyama T, Kuo CT, Creighton CJ, Mohila CA, Deneen B. Temporal Profiling of Astrocyte Precursors Reveals Parallel Roles for Asef during Development and after Injury. J Neurosci. 2016; 36:11904–11917. [PubMed: 27881777]

Dubey M, Bugiani M, Ridder MC, Postma NL, Brouwers E, Polder E, Jacobs JG, Baayen JC, Klooster J, Kamermans M, Aardse R, de Kock CP, Dekker MP, van Weering JR, Heine VM, Abbink TE, Scheper GC, Boor I, Lodder JC, Mansvelder HD, van der Knaap MS. Mice with megalencephalic leukoencephalopathy with cysts: a developmental angle. Ann Neurol. 2015; 77:114–131. [PubMed: 25382142]

Eng LF, Ghirnikar RS. GFAP and astrogliosis. Brain Pathol. 1994; 4:229–237. [PubMed: 7952264]

Freeman MR. Specification and morphogenesis of astrocytes. Science. 2010; 330:774–778. [PubMed: 21051628]

Fruttiger M. Development of the retinal vasculature. Angiogenesis. 2007; 10:77–88. [PubMed: 17322966]

Gallo V, Deneen B. Glial development: the crossroads of regeneration and repair in the CNS. Neuron. 2014; 83:283–308. [PubMed: 25033178]

Gerhardt H, Golding M, Fruttiger M, Ruhrberg C, Lundkvist A, Abramsson A, Jeltsch M, Mitchell C, Alitalo K, Shima D, Betsholtz C. VEGF guides angiogenic sprouting utilizing endothelial tip cell filopodia. J Cell Biol. 2003; 161:1163–1177. [PubMed: 12810700]

Gong S, Zheng C, Doughty ML, Losos K, Didkovsky N, Schambra UB, Nowak NJ, Joyner A, Leblanc G, Hatten ME, Heintz N. A gene expression atlas of the central nervous system based on bacterial artificial chromosomes. Nature. 2003; 425:917–925. [PubMed: 14586460]

Guo D, Zou J, Rensing N, Wong M. In Vivo Two-Photon Imaging of Astrocytes in GFAP-GFP Transgenic Mice. PLoS One. 2017; 12:e0170005. [PubMed: 28107381]

Ilja Boor PK, de Groot K, Mejaski-Bosnjak V, Brenner C, van der Knaap MS, Scheper GC, Pronk JC. Megalencephalic leukoencephalopathy with subcortical cysts: an update and extended mutation analysis of MLC1. Hum Mutat. 2006; 27:505–512. [PubMed: 16652334]

Jain RK, di Tomaso E, Duda DG, Loeffler JS, Sorensen AG, Batchelor TT. Angiogenesis in brain tumours. Nat Rev Neurosci. 2007; 8:610–622. [PubMed: 17643088]

John Lin CC, Yu K, Hatcher A, Huang TW, Lee HK, Carlson J, Weston MC, Chen F, Zhang Y, Zhu W, Mohila CA, Ahmed N, Patel AJ, Arenkiel BR, Noebels JL, Creighton CJ, Deneen B. Identification of diverse astrocyte populations and their malignant analogs. Nat Neurosci. 2017; 20:396–405. [PubMed: 28166219]

Leegwater PA, Yuan BQ, van der Steen J, Mulders J, Konst AA, Boor PK, Mejaski-Bosnjak V, van der Maarel SM, Frants RR, Oudejans CB, Schutgens RB, Pronk JC, van der Knaap MS. Mutations of MLC1 (KIAA0027), encoding a putative membrane protein, cause megalencephalic

Author Manuscript Author Manuscript Author Manuscript Author Manuscript

leukoencephalopathy with subcortical cysts. Am J Hum Genet. 2001; 68:831–838. [PubMed: 11254442]

Liddelow SA, Barres BA. Regeneration: Not everything is scary about a glial scar. Nature. 2016; 532:182–183. [PubMed: 27027287]

Lim DA, Alvarez-Buylla A. The Adult Ventricular-Subventricular Zone (V-SVZ) and Olfactory Bulb (OB) Neurogenesis. Cold Spring Harb Perspect Biol. 2016; 8

McCarty JH. Cell adhesion and signaling networks in brain neurovascular units. Curr Opin Hematol. 2009; 16:209–214. [PubMed: 19318941]

McCarty JH, Lacy-Hulbert A, Charest A, Bronson RT, Crowley D, Housman D, Savill J, Roes J, Hynes RO. Selective ablation of alphav integrins in the central nervous system leads to cerebral hemorrhage, seizures, axonal degeneration and premature death. Development. 2005; 132:165–176. [PubMed: 15576410]

Metin C, Vallee RB, Rakic P, Bhide PG. Modes and mishaps of neuronal migration in the mammalian brain. J Neurosci. 2008; 28:11746–11752. [PubMed: 19005035]

Muoio V, Persson PB, Sendeski MM. The neurovascular unit - concept review. Acta Physiol (Oxf). 2014; 210:790–798. [PubMed: 24629161]

Nagelhus EA, Mathiisen TM, Ottersen OP. Aquaporin-4 in the central nervous system: cellular and subcellular distribution and coexpression with KIR4.1. Neuroscience. 2004; 129:905–913. [PubMed: 15561407]

Noctor SC, Flint AC, Weissman TA, Dammerman RS, Kriegstein AR. Neurons derived from radial glial cells establish radial units in neocortex. Nature. 2001; 409:714–720. [PubMed: 11217860]

Ozduman K, Pober BR, Barnes P, Copel JA, Ogle EA, Duncan CC, Ment LR. Fetal stroke. Pediatr Neurol. 2004; 30:151–162. [PubMed: 15033196]

Pekny M, Nilsson M. Astrocyte activation and reactive gliosis. Glia. 2005; 50:427–434. [PubMed: 15846805]

Ribotta MG, Menet V, Privat A. Glial scar and axonal regeneration in the CNS: lessons from GFAP and vimentin transgenic mice. Acta Neurochir Suppl. 2004; 89:87–92. [PubMed: 15335106]

Segarra M, Kirchmaier BC, Acker-Palmer A. A vascular perspective on neuronal migration. Mech Dev. 2015; 138(Pt 1):17–25. [PubMed: 26192337]

Shinozaki Y, Shibata K, Yoshida K, Shigetomi E, Gachet C, Ikenaka K, Tanaka KF, Koizumi S. Transformation of Astrocytes to a Neuroprotective Phenotype by Microglia via P2Y1 Receptor Downregulation. Cell Rep. 2017; 19:1151–1164. [PubMed: 28494865]

Sloan SA, Barres BA. Mechanisms of astrocyte development and their contributions to neurodevelopmental disorders. Current opinion in neurobiology. 2014; 27:75–81. [PubMed: 24694749]

Sofroniew MV. Molecular dissection of reactive astrogliosis and glial scar formation. Trends Neurosci. 2009; 32:638–647. [PubMed: 19782411]

Szymczak AL, Workman CJ, Wang Y, Vignali KM, Dilioglou S, Vanin EF, Vignali DA. Correction of multi-gene deficiency in vivo using a single 'self-cleaving' 2A peptide-based retroviral vector. Nat Biotechnol. 2004; 22:589–594. [PubMed: 15064769]

Tchaicha JH, Reyes SB, Shin J, Hossain MG, Lang FF, McCarty JH. Glioblastoma angiogenesis and tumor cell invasiveness are differentially regulated by beta8 integrin. Cancer Res. 2011; 71:6371–6381. [PubMed: 21859829]

Toutounchian JJ, Pagadala J, Miller DD, Baudry J, Park F, Chaum E, Yates CR. Novel Small Molecule JP-153 Targets the Src-FAK-Paxillin Signaling Complex to Inhibit VEGF-Induced Retinal Angiogenesis. Mol Pharmacol. 2017; 91:1–13. [PubMed: 27913654]

Turner DA, Adamson DC. Neuronal-astrocyte metabolic interactions: understanding the transition into abnormal astrocytoma metabolism. J Neuropathol Exp Neurol. 2011; 70:167–176. [PubMed: 21293295]

van der Knaap MS, Barth PG, Stroink H, van Nieuwenhuizen O, Arts WF, Hoogenraad F, Valk J. Leukoencephalopathy with swelling and a discrepantly mild clinical course in eight children. Ann Neurol. 1995; 37:324–334. [PubMed: 7695231]

Author Manuscript Author Manuscript Author Manuscript Author Manuscript

Xu H, Yang Y, Tang X, Zhao M, Liang F, Xu P, Hou B, Xing Y, Bao X, Fan X. Bergmann glia function in granule cell migration during cerebellum development. Mol Neurobiol. 2013; 47:833–844. [PubMed: 23329344]

Yang SM, Alvarez DD, Schinder AF. Reliable Genetic Labeling of Adult-Born Dentate Granule Cells Using Ascl1 CreERT2 and Glast CreERT2 Murine Lines. J Neurosci. 2015; 35:15379–15390. [PubMed: 26586824]

Yao Y, Chen ZL, Norris EH, Strickland S. Astrocytic laminin regulates pericyte differentiation and maintains blood brain barrier integrity. Nat Commun. 2014; 5:3413. [PubMed: 24583950]

Zhang Y, Barres BA. Astrocyte heterogeneity: an underappreciated topic in neurobiology. Curr Opin Neurobiol. 2010; 20:588–594. [PubMed: 20655735]

Zhao Z, Nelson AR, Betsholtz C, Zlokovic BV. Establishment and Dysfunction of the Blood-Brain Barrier. Cell. 2015; 163:1064–1078. [PubMed: 26590417]

Author Manuscript Author Manuscript Author Manuscript Author Manuscript

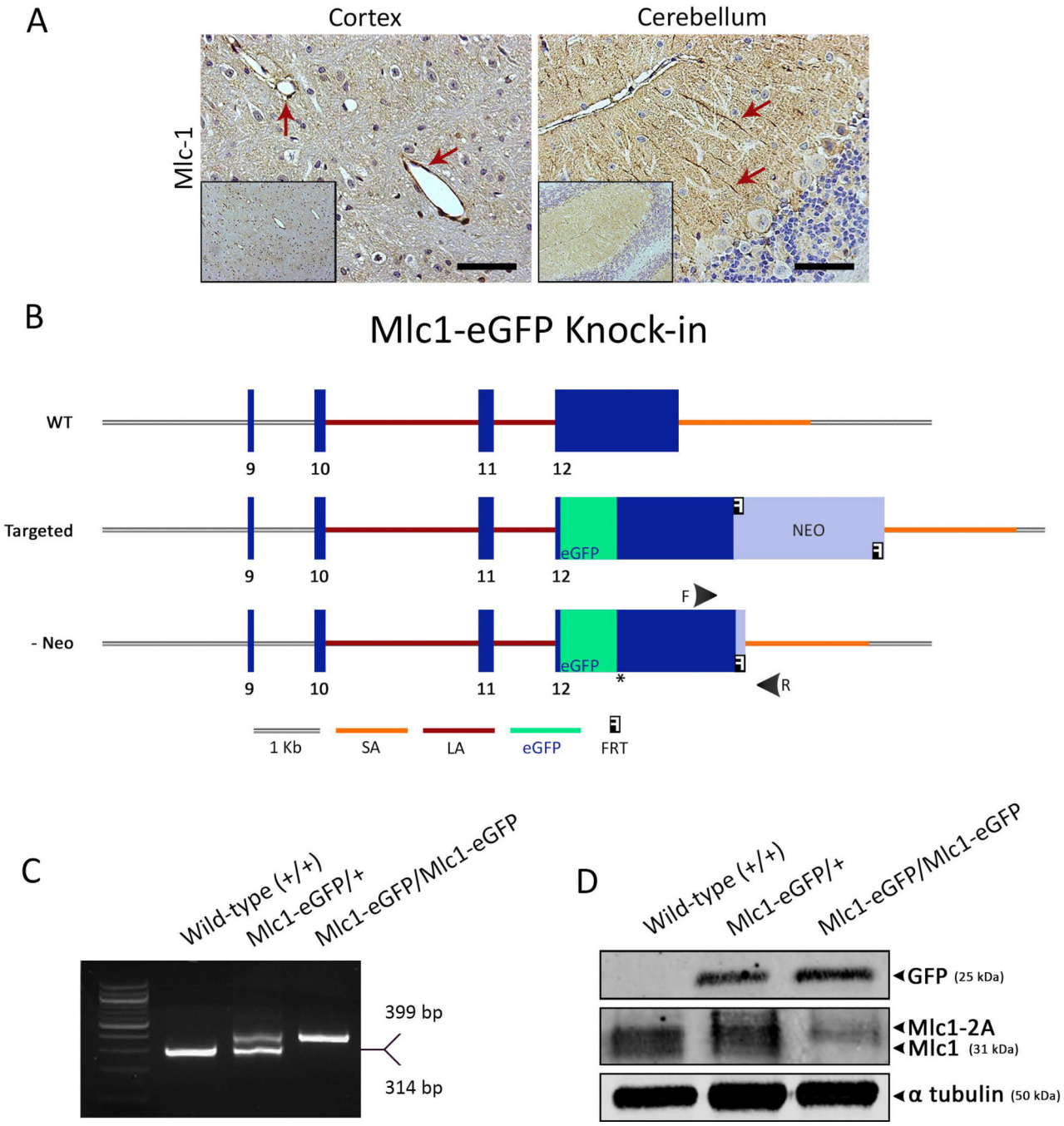

Fig 1. Generation and characterization of the Mlc1-eGFP knock-in mouse model

(A); Immunohistochemical analysis of adult mouse brain sections using an anti-Mlc1 antibody reveals Mlc1 protein expression localize around blood vessels in the cortex (red arrows, left panel) as well as in Bergmann glial processes in the cerebellum (red arrows, right panel). Inserts are lower magnification images. Scale bars: 500 μm. Control IgG immunostains did not show immunoreactivity (S1 Fig). **(B);** Strategy to regulate eGFP via the endogenous Mlc1 promoter based on T2A ribosome skipping. The schematic shows the 3' region of the endogenous murine Mlc1 locus (top) containing exons 9 to 12, and the

Author Manuscript Author Manuscript Author Manuscript Author Manuscript

targeted Mlc1 locus before (middle) and after (lower) Flp-mediated excision of the inverted Neomycin cassette in ES cells. The asterisk indicates the TGA termination codon in Mlc1 exon 12, located downstream of the eGFP cDNA sequence. Abbreviations, SA: short arm of the targeting vector, LA: long arm of the targeting vector. **(C);** Genotyping using PCR and genomic DNA isolated from tail snips distinguishes wild type, heterozygous (Mlc1-eGFP/+) and homozygous (Mlc1-eGFP/Mlc1-eGFP) mice. The PCR product for the wild-type allele is 314 bp. After Neo deletion, one FRT site remains (85 bp). A higher molecular weight band with a size of 399 bp indicates the knock-in allele. **(D);** Detergent-soluble whole brain lysates from wild type, heterozygous and homozygous mice (P30) were analyzed by immunoblotting with anti-GFP and anti-Mlc1 antibodies. Anti-tubulin immunoblotting was performed as a loading control.

Author Manuscript Author Manuscript Author Manuscript Author Manuscript

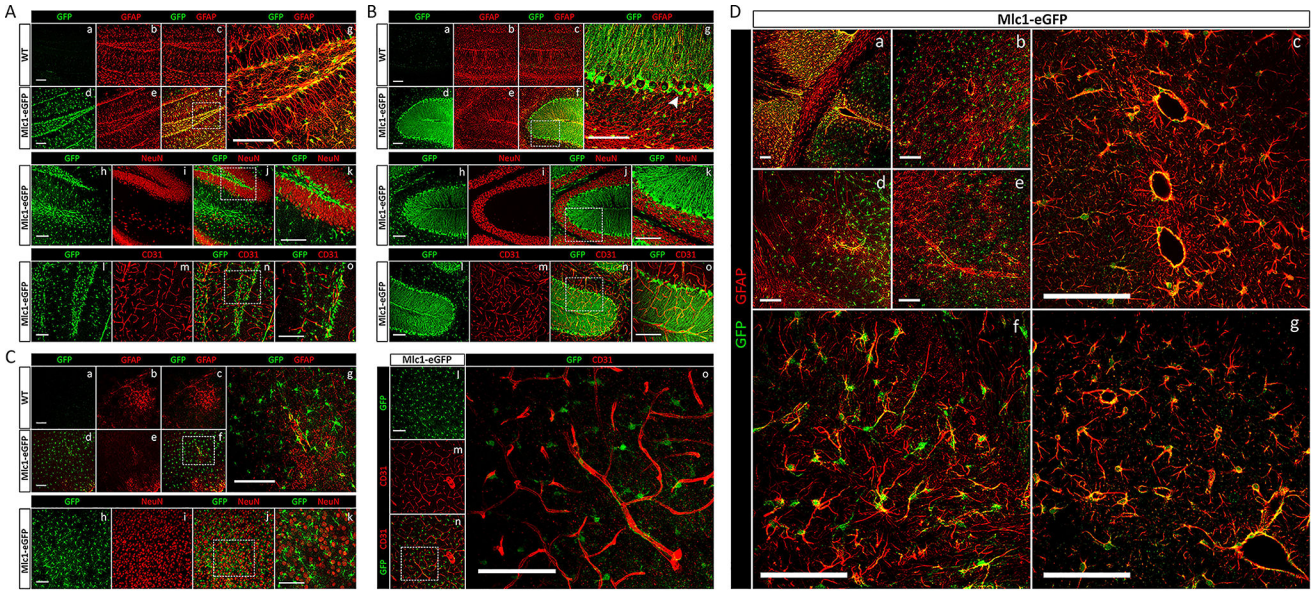

Fig 2. The endogeneous Mlc1 gene regulates eGFP expression in perivascular astrocytes of the adult brain

(A); Double immunofluorescence labeling reveals co-localization of GFAP with eGFP in astrocytes within the adult hippocampus of wild type (WT) and heterozygous (Mlc1-eGFP/+) mice (a–c and d–g, respectively). Note that neurons (NeuN, h–k) and endothelial cells (CD31, l–o) are not positive for eGFP expression. **(B);** Immunofluorescence with anti-GFAP and anti-eGFP reveals co-localization in Bergmann glia the adult cerebellum (a–g). Glial cell bodies (white arrow) are immunoreactive for eGFP only, but their radial processes show both GFAP and eGFP expression. There is no detectable overlap in expression for eGFP and neuronal (NeuN, h–k) and vascular endothelial cell markers (CD31, l–o). However, note the close apposition of the eGFP-expressing glial processes and CD31-expressing blood vessels. **(C);** GFAP processes originating from eGFP-expressing cell bodies identify astrocytes in the adult cerebral cortex (a–g), while neither neurons (h–k) nor endothelial cells (l–o) show eGFP co-localization. Scale bars: 100 μm. **(D);** Analysis of eGFP and GFAP expression in the adult cerebral cortex. There is obvious co-expression of eGFP and GFAP in perivascular astrocytes (a–g). Note that eGFP is expressed in astrocyte cell bodies and processes, whereas GFAP is expressed only in cell processes. Scale bars: 100 μm.

Author Manuscript Author Manuscript Author Manuscript Author Manuscript

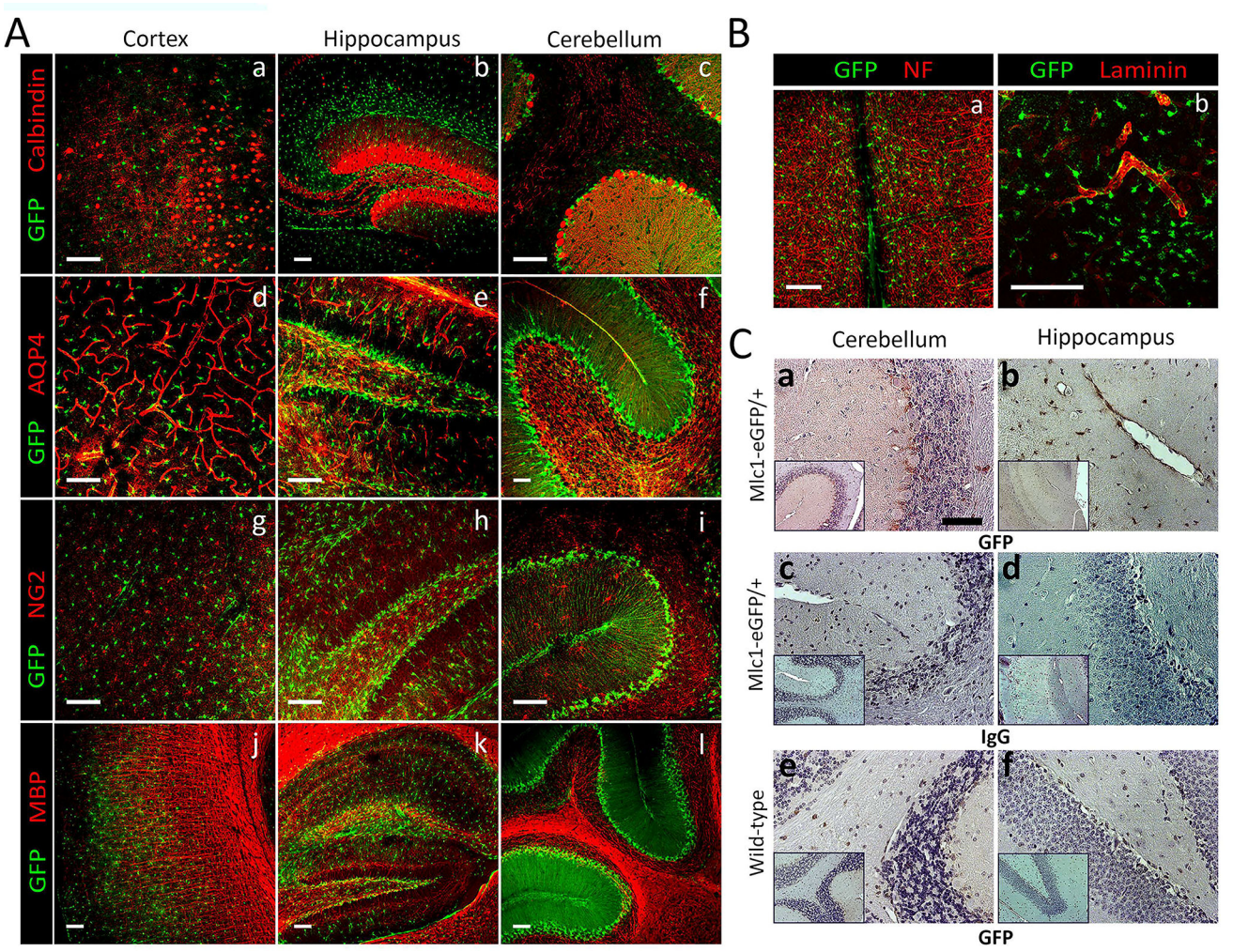

Fig 3. Analysis of eGFP expression in neuronal, glial and vascular cell types of the adult brain

(A); Anti-GFP antibodies were used in combination with anti-calbindin (a–c), anti-aquaporin-4 (AQP4) (d–f), anti-neuroglial antigen 2 (NG2) (g–i), and anti-myelin basic protein (MBP) (**j–l**) were used to label sections from the P30 cortex, hippocampus, and cerebellum. **(B);** Double immunolabeling for eGFP and Neurofilament (NF) in the hippocampus (a) and eGFP and laminin in the cortex (a, b). **(C);** Anti-GFP versus control IgG antibodies reveal specific eGFP expression in the P30 cerebellum and hippocampus of Mlc1-eGFP/+ heterozygous mice (c, d). EGFP expression is not detected in wild type control brain sections (e, f). White scale bars: 100 μm, black scale bars: 500 μm.

Author Manuscript Author Manuscript Author Manuscript Author Manuscript

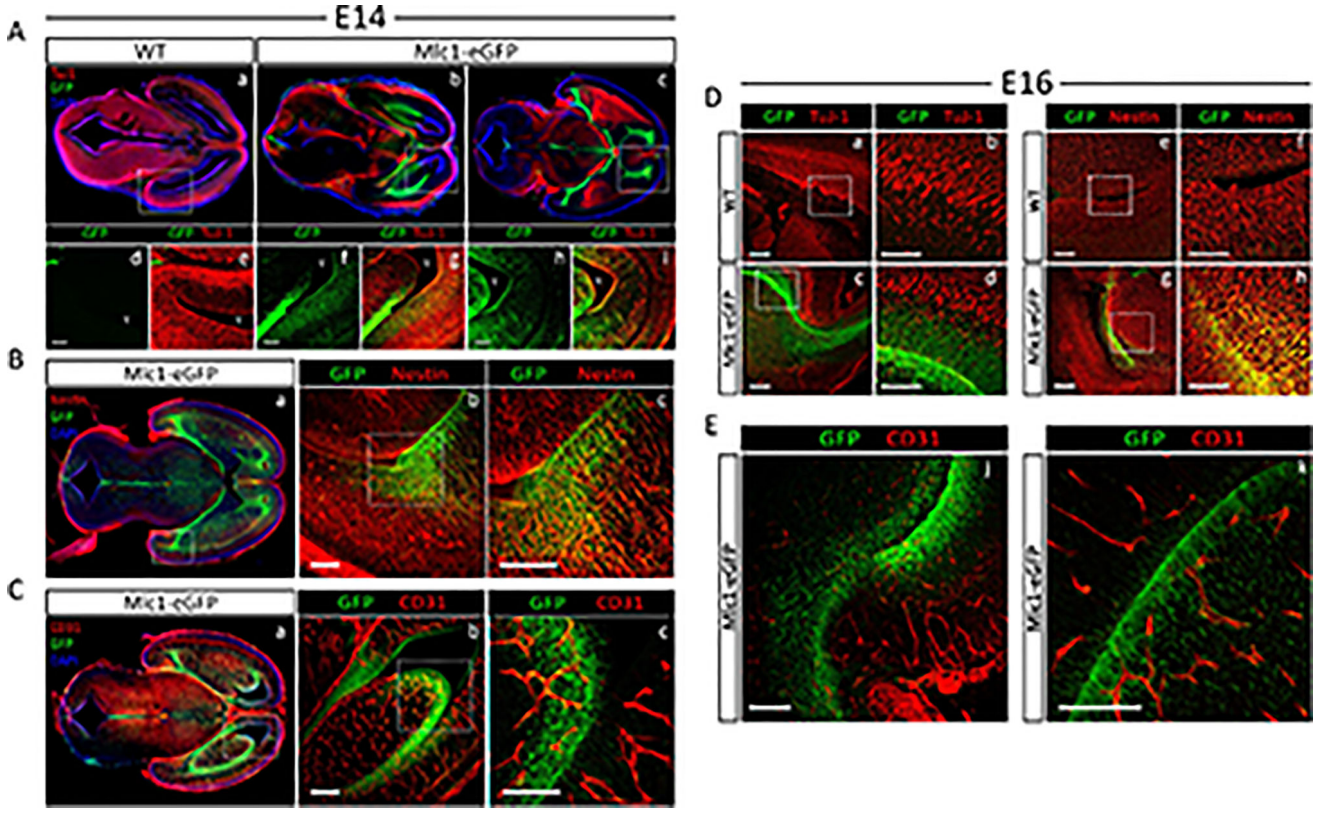

Fig 4. Dynamic patterns of eGFP expression in the embryonic mouse brain

(A); Analysis of eGFP and Tuj1 expression patterns in wild type (WT) and heterozygous (Mlc1-eGFP) E14 horizontal brain slices (a–c). Anti-GFP and Anti-Tuj1 double immunofluorescence labeling shows clear demarcation between newly differentiated neurons (red) and cells expressing eGFP (d–i). Boxed regions in a, b, c are shown at higher magnification in d–i. **(B);** Nestin and eGFP double immunofluorescence analyses in E14 embryonic brains reveal clear co-localization in periventricular regions (a–c). Boxed regions in a, b are shown at higher magnification in c. **(C);** Anti-CD31 and anti-GFP double immunofluorescent labeling reveals non-overlapping patterns of CD31-expressing blood vessels and eGFP-expressing neuroepithelial cells in the E14 brain (a–c). **(D);** Double immunofluorescence labeling for eGFP/Tuj1 (a–d) and eGFP/Nestin (e–h) in horizontal brain sections from E16 wild type (WT) control and heterozygous (Mlc1-eGFP) embryos. Boxed regions in a, c, e, g are shown at higher magnification in b, d, f, h. **(E);** Anti-CD31 and anti-GFP double labeling of E16 embryonic brain sections from wild type and heterozygous littermates reveals close contacts between perivascular cells (green) and blood vessels (red) (j, k). Scale bars: 100 μm.

Author Manuscript
Author Manuscript
Author Manuscript
Author Manuscript

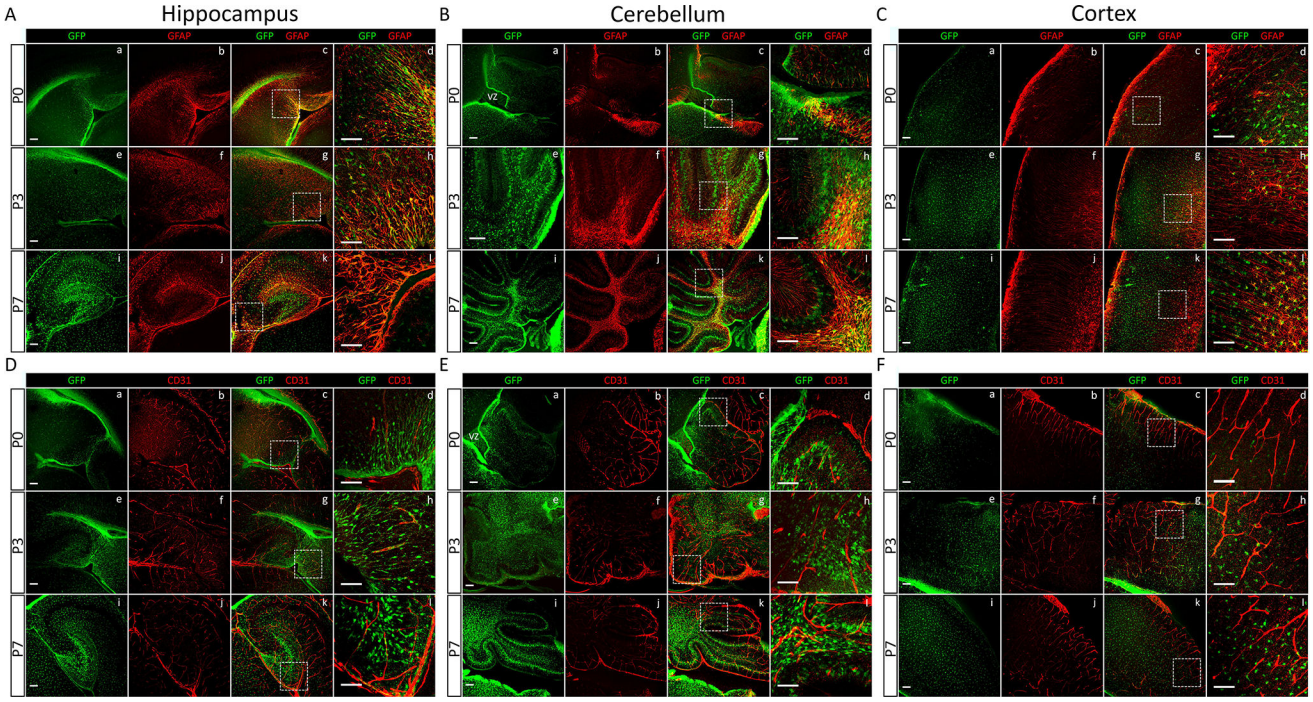

Fig 5. Spatiotemporal changes in eGFP expression in the neonatal mouse brain

(A–C); Co-localization analysis of eGFP and GFAP identifies sub-populations of astrocytes in the developing hippocampus (A), cerebellum (B), and the cortex (C) of Mlc1-eGFP/+ heterozygous pups at post-natal days P0 (a–d), P3 (e–h), and P7 (i–l). **(D–F);** Co-localization analysis of eGFP and CD31 in the developing hippocampus (D), cerebellum (E), and the frontal cortex (F) of Mlc1-eGFP/+ mice at postnatal days P0 (a–d), P3 (e–h), and P7 (i–l). Boxed regions in c, g, h are shown at higher magnification in d, h, i. Scale bars: 100 μm.

Author Manuscript Author Manuscript Author Manuscript Author Manuscript

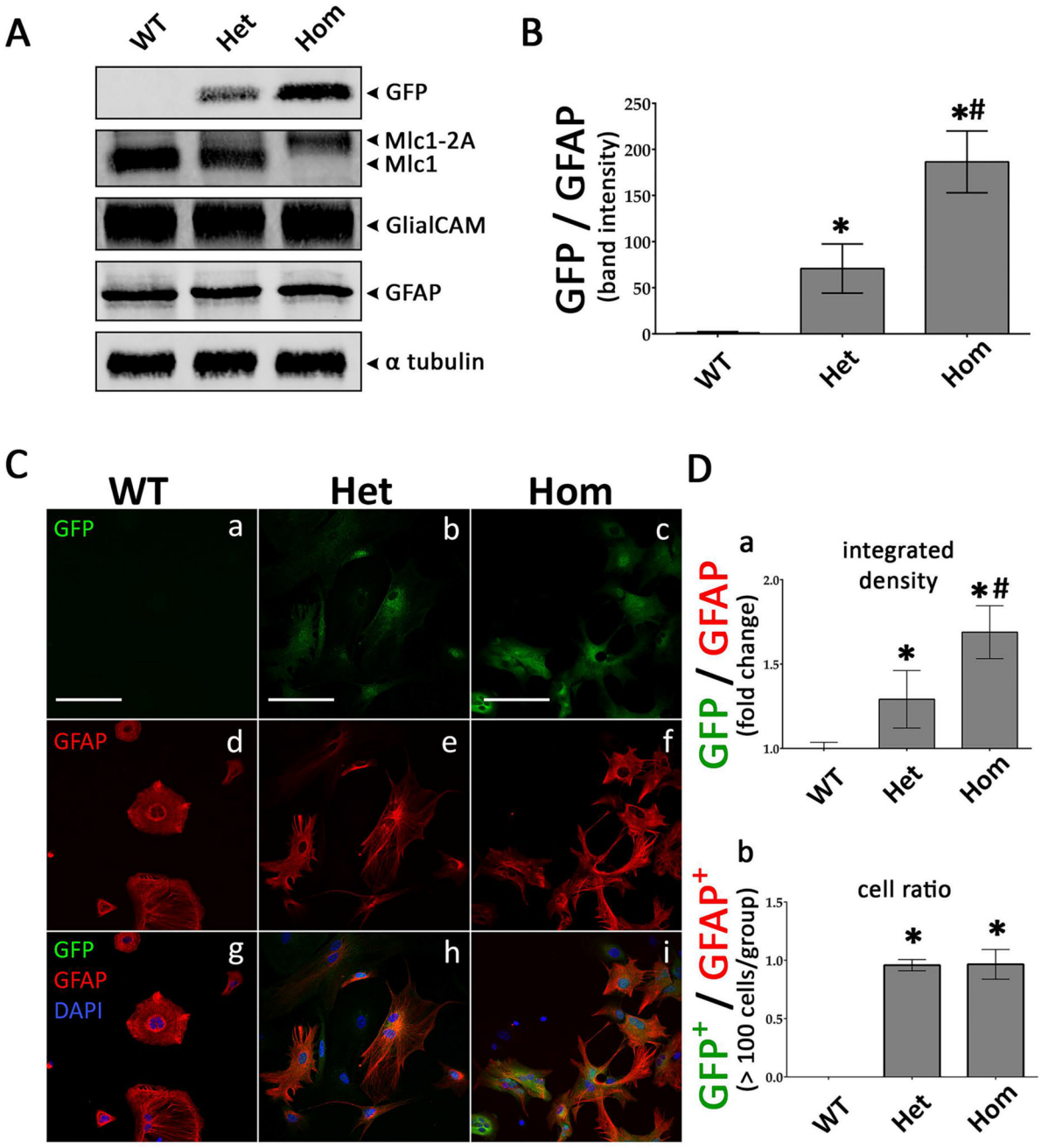

Fig 6. Primary brain astrocytes cultured from Mlc1-eGFP knock-in mice express eGFP and Mlc1

(A); Detergent-soluble lysates from cultured astrocytes cultured from wild-type, Mlc1-eGFP/+ heterozygous, and Mlc1-eGFP/ Mlc1-eGFP homozygous neonates were analyzed for eGFP, Mlc1, GlialCAM, GFAP, and α-tubulin protein expression (loading control) by immunoblotting. **(B);** Analysis of eGFP and GFAP protein levels reveal no detectible eGFP in wild type cells, whereas astrocytes from heterozygous and homozygous pups were positive for eGFP (n =3; *,#P < 0.01). **(C);** Immunofluorescence labeling shows overlapping eGFP (a–c) and GFAP (d–f) expression in cultured astrocytes from heterozygous and

homozygous neonates, compared to wild type controls (panels g–i). Scale bars: 100 μm. **(D);** Expression of eGFP and GFAP proteins in cultured astrocytes as determined by integrated density (ID) levels of eGFP positive cells normalized to GFAP (a, n = 3 experiments, with ≥ 5 fields of view; *,#P < 0.01). Additionally, cells positive for eGFP were normalized to those that were also GFAP positive (b, n > 100 cells, *P < 0.01). Data represent mean ± SD.

Author Manuscript Author Manuscript Author Manuscript Author Manuscript

Author Manuscript Author Manuscript Author Manuscript Author Manuscript

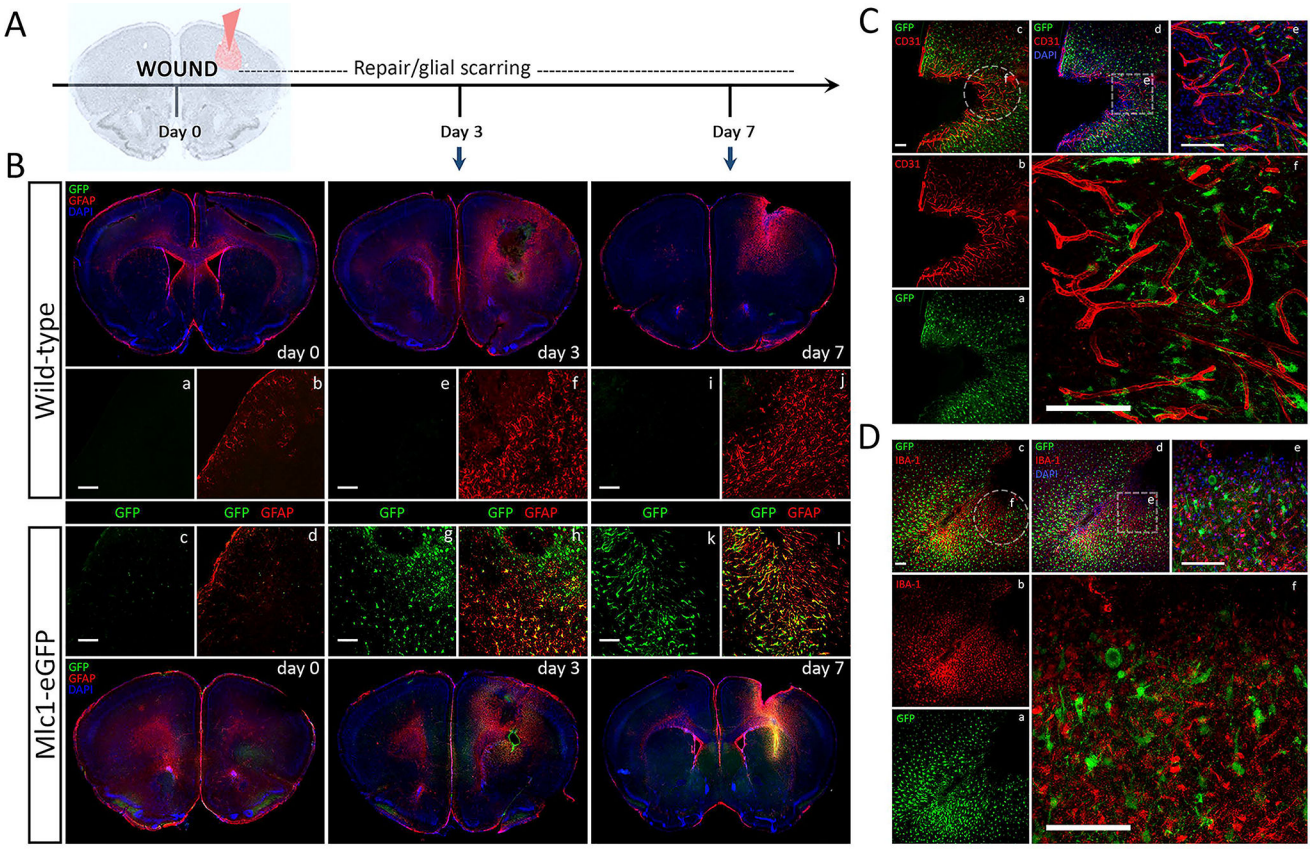

Fig 7. Mlc1-eGFP expression in activated in astrocytes in response to brain injury

(A); Schematic depicting the experimental strategy for the cortical wound model with analysis at 3 days and 7 days post-injury. **(B);** At 3 and 7 days after the stab wound, Mlc1-eGFP/+ and wild type control brains were removed, sectioned through the site of injury, and immunofluorescently labeled with anti-GFP and anti-GFAP antibodies. Non-injured control brains (wild type and heterozygous) were sectioned at day 0 for comparison (a–d). Reactive astrogliosis, as revealed by coincident expression of GFAP, is evident at three days post-injury (e–h) and is more obvious at seven days after injury (i–j). Note that the eGFP expression coincides with upregulation of GFAP. **(C);** EGFP and CD31 double immunofluorescent staining of Mlc1-eGFP/+ heterozygote mice at day 7 reveals perivascular patterns of $eGFP^{+}$ cells (a–f). **(D);** Anti-GFP and anti-IBA-1 double labeling of Mlc1-eGFP/+ heterozygote mice at day 7 reveals reactive microglial cells that do not express eGFP (a–f). For these experiments three mice were analyzed per time point and genotype). Scale bars: 100 μm.

Author Manuscript
Author Manuscript
Author Manuscript
Author Manuscript

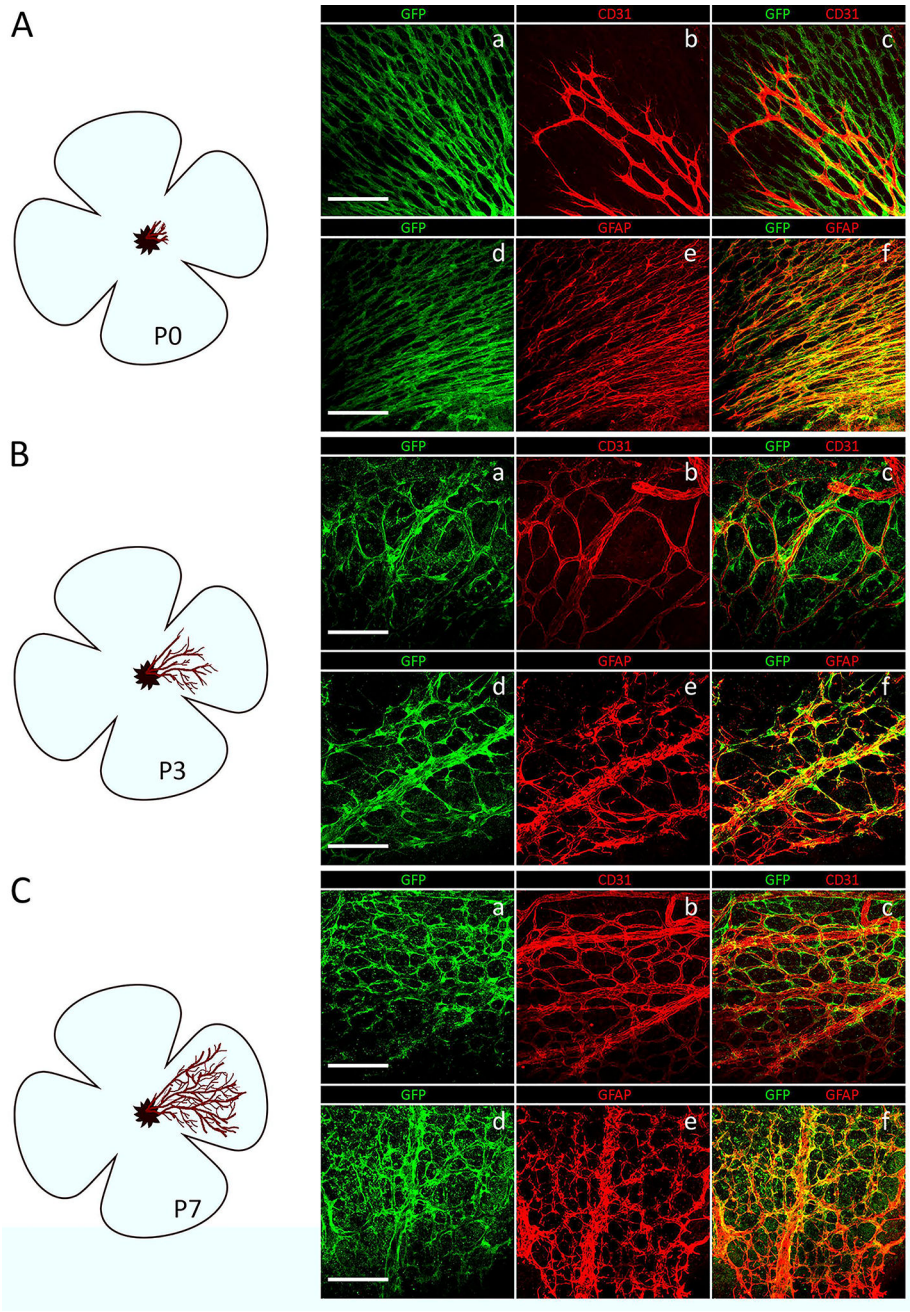

Fig 8. Analysis of Mlc1-eGFP expression in the developing mouse retina

(A–C); Double immunofluorescence analysis with anti-GFP antibody in combination with anti-CD31 (a–c) or anti-GFAP (d–f) antibodies using flat-mounted mouse retinas at P0 **(A)**, P3 **(B)**, and P7 **(C)**. Note the striking overlap of eGFP/GFAP expression in the P0 retina, defining the astrocytic network along which angiogenic blood vessels migrate to form the primary retinal vascular plexus. As retinal vascular development progresses at days 3 and 7, eGFP expression becomes more focally defined around angiogenic blood vessels. In anti-GFP and anti-CD31 immunolabeled P3 and P7 retina flat mounts, eGFP-expressing

perivascular astrocytes show close juxtaposition with angiogenic blood vessels. Scale bars: 100 μm.

Author Manuscript Author Manuscript Author Manuscript Author Manuscript

Author Manuscript Author Manuscript Author Manuscript Author Manuscript

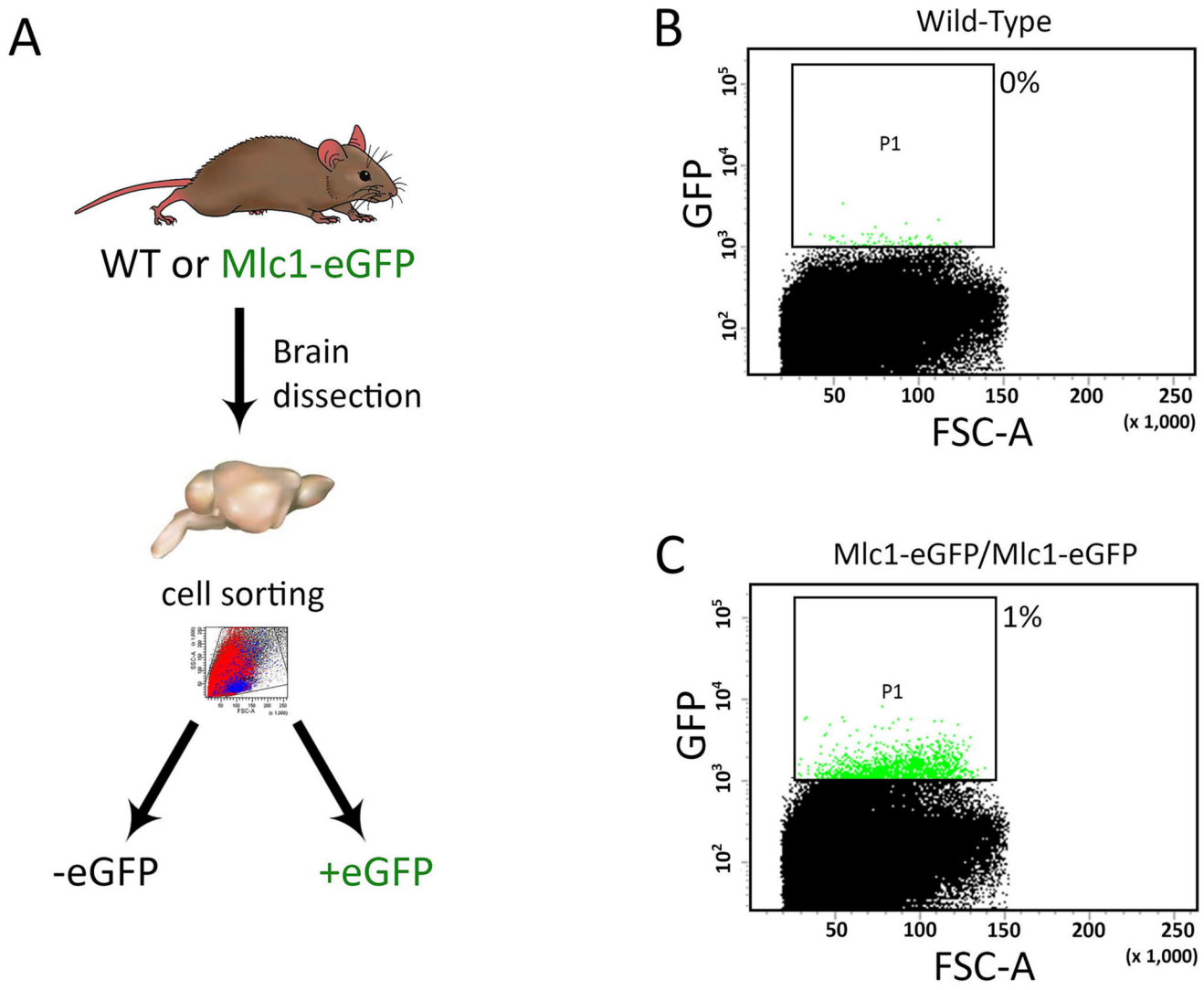

Fig 9. Fractionation of eGFP-expressing cells from the adult brain

(A); Model depicting the fractionation of $EGFP^+$ cell populations from cerebral cortices of Mlc1-eGFP littermates. **(B, C)**; $EGFP^+$ cells were fractionated from bulk cell suspensions prepared from dissociated cerebral cortices dissected from P30 wild type control **(B)** and Mlc1-eGFP homozygous littermates **(C)**. Note that 1% of the bulk cell population from homozygous cortices expresses detectable levels of eGFP, whereas the wild type cortices lack eGFP-expressing cells.